Published by Avanti Publishers

International Journal of Architectural Engineering Technology

ISSN (online): 2409-9821

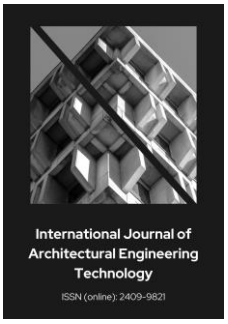

Experimental and Numerical Investigation of Downburst-Like Wind Fields: Spatiotemporal Characteristics and Turbulence Behavior from Wind Tunnel Experiments and CFD Simulation

Zhipeng Wang[1], Lunhai Zhi[1,*], Bowen Yan[2] and Wei Guo[1]

[1]*College of Civil Engineering, Hefei University of Technology, Hefei, Anhui 230009, China*

[2]*Key Laboratory of New Technology for Construction of Cities in Mountain Area (Ministry of Education), School of Civil Engineering, Chongqing University, Chongqing 400045, China*

ARTICLE INFO

Article Type: Research Article

Academic Editor: Fatemeh Rezaei

Keywords:
Turbulence structure
Downburst wind field
Wind tunnel experiment
Non-stationary wind characteristics
Wind engineering and structural wind loads

Timeline:
Received: February 02, 2026
Accepted: March 25, 2026
Published: April 20, 2026

Citation: Wang Z, Zhi L, Yan B, Guo W. Experimental and numerical investigation of downburst-like wind fields: Spatiotemporal characteristics and turbulence behavior from wind tunnel experiments and CFD simulation. Int J Archit Eng Technol. 2026; 13(1): 84-98.

DOI: https://doi.org/10.15377/2409-9821.2026.13.5

ABSTRACT

Downburst is an extreme wind event caused by a thunderstorm downdraft that impinges upon the ground and subsequently forms a near-ground gust front, resulting in substantial economic losses and structural damage. Due to its pronounced discrepancies from synoptic winds, constructing downburst wind field models is crucial for the refined assessment of wind loads and structural safety. This study investigates the spatiotemporal distribution characteristics of downburst-like wind fields based on active-controlled wind tunnel tests and numerical approach utilizing the large-eddy simulation (LES). The work primarily focuses on the disparities regarding mean and fluctuating wind characteristic between stationary flows and non-stationary outflows with various gust durations. The findings demonstrate a substantial concordance between the numerically simulated downburst wind fields and the experimental results. Compared with the stationary flows, the non-stationary cases exhibit pronounced time-varying characteristics across the mean wind profile and turbulence parameters including turbulence intensity, integral length scales, and fluctuating wind velocity spectra. Furthermore, an increase in the gust duration of non-stationary flows leads to a reduction in the peak time-varying mean velocity, while weakening the non-Gaussian features in the residual fluctuation and suppressing the peak energy of evolutionary power spectral density. The insights from this study are intended to deepen the comprehensive understanding of downburst wind field characteristics.

*Corresponding Author
Email: zhilunhai1979@163.com
Tel: +(86) 18627741286

1. Introduction

Thunderstorm downburst is a localized strong wind event capable of generating extreme velocities, thereby posing severe threats to civil and electrical infrastructure in non-typhoon cyclone regions [1-4]. Such extreme wind speeds are driven by gust fronts, generated when a thunderstorm downdraft impinges on the ground and radiates outward [5, 6]. Distinct from synoptic winds characterized by conventional boundary layer profiles, downburst outflows exhibit a unique "nose-shaped" vertical profile, where the maximum velocity is located close to the ground. Nevertheless, considerable existing studies primarily rely on synoptic wind models for the evaluation of structural wind loads [7-9], which may lead to unfavorable implications for structural design. Consequently, a comprehensive understanding of the spatiotemporal evolution of downburst wind fields is essential for advancing rational wind-resistant designs and formulating relevant code provisions.

With growing concern over the hazards induced by downbursts, substantial effort has been devoted to investigating their wind-field characteristics and associated structural wind effects. Currently, the primary research methodologies involve field measurements, wind-tunnel experiments, and numerical simulations. Field monitoring is widely regarded as the most direct and reliable method for acquiring real data and can provide a reference benchmark for experiments and simulations. Existing field measurement projects include the Northern Illinois Meteorological Research on Downbursts (NIMROD) project, the Classify, Locate and Avoid Wind Shear (CLAWS) project, and the "Wind and Ports" project [10-12], among others. Given the high spatiotemporal unpredictability of downbursts, acquiring reliable field observational data remains a significant challenge [13]. To overcome this limitation, researchers have devoted substantial efforts to reproducing downburst outflows via experimental techniques and computational fluid dynamics simulations (CFD), predominantly utilizing impinging jets (IJ), multi-fan arrays, and multi-blade systems [14-20]. By employing large-scale downburst simulator in the Wind Engineering, Energy, and Environment (WindEEE) Dome at Western University, Canepa *et al*. [21] investigated and quantified the complex interactions among downbursts, ABL flows, and thunderstorm translation. Utilizing the identical facility, Canepa *et al*. [22] investigated the influence of surface roughness on the profiles of wind velocity and turbulence intensity. While such large-scale simulation devices can reproduce the spatiotemporal evolution characteristics of three-dimensional flow fields, they simultaneously introduce complexities into the evaluation of structural aerodynamic responses [23]. Additionally, Yan *et al*. [24] refined the empirical model of downburst wind fields using a small-scale IJ model at Beijing Jiaotong University. However, such small-scale setups may fail to replicate the high-Reynolds-number flow conditions achievable in the aforementioned large-scale facilities. An alternative methodology for replicating downburst outflows involves modifying the atmospheric boundary layer wind tunnel by adding multi-fan or multi-blade devices. Li *et al*. [25] used a multi-fan wind tunnel at Tamkang University to compare the aerodynamic characteristics of a high-rise building under ABL winds and stationary thunderstorm downburst. Babu *et al*. [26] used a similar facility to evaluate compare the effects of translational, gust-front, and transient downbursts on the wind load characteristics of high-rise buildings. However, the electrical or manual modulation of multiple independent fans complicates the simulation of non-stationary transient gusts. To address this, Butler and Kareem [27] developed a simplified Flat Plate at a High Incidence (FPHI) setup based on the concept of flow redirection, successfully simulating the transient wind effects on a prismatic model. Inspired by this, Aboutabikh *et al*. [28] developed a system incorporating multiple louvers in the subsonic wind tunnel at Ryerson University, calibrated via CFD simulations. Le and Caracoglia [29] utilized a similar apparatus to validate the effectiveness of reproducing stationary and non-stationary downburst outflows. In a recent study, Yuan *et al*. [30, 31] advanced the above concept by introducing an active multi-blade system with adjustable rotation angles and timing. Utilizing a combination of experimental tests and CFD simulations, they successfully generated the primary vortex of a two-dimensional downburst that matches full-scale events. Furthermore, the simulated stationary outflows and transient gusts have been applied to assess the wind effects on high-rise buildings and wind turbines [32, 33]. A review of the literature indicates that the active-controlled multi-blade systems can effectively reproduce 2D downburst flow fields through the modifications to conventional boundary layer wind tunnels. These setups are capable of simulating both stationary flows with distinct profiles and non-stationary flows with time-dependent intensification. In this process, the rotation rate of the blades determines the velocity variation rate and the resultant gust duration. Nevertheless, the influence of these parameters on non-stationary wind field properties remains insufficiently explored. As demonstrated by Chen [34], the variations in gust duration may exert a pronounced influence on the magnitude of wind-induced responses.

Yan *et al*. [32] observed that the wind pressure overshoot ratios on a wind turbine nacelle are positively correlated with wind acceleration. Moreover, the comparative analysis of statistical characteristics between stationary and non-stationary wind fields remains insufficient. Therefore, it is imperative to conduct a comprehensive statistical analysis of stationary outflows and non-stationary winds with varying gust durations.

The primary objective of this study is to gain a deeper understanding of the temporal evolution of wind field characteristics during downburst events through both wind tunnel test and numerical simulation. The validity and potentials of the numerical simulations are evaluated based on experimental results. The investigation is focused on the variations in mean and fluctuating wind characteristic parameters between stationary and non-stationary flow conditions. Wind profiles, probability density distributions, turbulence intensity, turbulence integral scale, and power spectral density are presented and discussed in detail. Section 2 introduces the experimental setup and the parameter settings utilized in the numerical simulations; Section 3 presents the results concerning the mean and fluctuating wind characteristics; and Section 4 summarizes the principal conclusions of the study.

2. Data and Methodology

2.1. Wind Tunnel Tests

The experiments are conducted in the open-circuit wind tunnel (CQU-1) at Chongqing University. The total length (L) of the test section is 15 m, with a cross-sectional area measuring 2.4 m in width (B) and 1.8 m in height (H). By modulating the high-power fan, the maximum achievable wind velocity within the working chamber is 30 m/s. The downburst-like outflow in this experiment is generated by the active-controlled multi-blade system (AMBS) device (Fig. **1**). The AMBS setup measures 2250 mm in width and 600 mm in depth, consisting of an aluminum alloy structural frame, lateral supports, and an array of four blades. Each blade is constructed from a plastic framework reinforced by wooden ribs, with dimensions of 2000 mm (length) × 500 mm (width) × 10 mm (thickness). The rotation configurations of the blades are primarily modulated by motors driven by independent controllers, and the integrated operation is managed by a proprietary software platform. This facility has been thoroughly tested and calibrated in prior investigations [30-32], demonstrating its capacity and potential for simulating thunderstorm outflows. In the current study, the experimental wind speed is set to 12 m/s. The wind field measurements are taken at a location 3 m downstream of the AMBS device, and the velocities data are acquired using a Cobra probe anemometer. Each measurement is sampled for a duration of 15 s at a resolution of 250 Hz. Given the two-dimensional nature of the generated flow field, the analysis focuses exclusively on the streamwise velocity time histories. Stationary and non-stationary outflows are generated by static and dynamically rotating blade configurations, respectively. The corresponding time histories for the blade rotation are depicted in Fig. (**2**), where the maximum rotation angle is 36°. For the static blade configuration, sampling of the data commences 3 seconds after the flow stabilization, with the blade angle held constant. In the dynamic blade configuration, the temporal evolution of the velocity is primarily governed by variations in the blade angle and the specific time intervals (ΔT and Δt). This study employs three distinct durations for ΔT (0.2 s, 0.5 s, and 0.8 s), while Δt is consistently maintained at 0.1 s, to replicate nonstationary downburst characterized by varying gust durations. To satisfy the similarity criteria between the wind tunnel model and full-scale downburst events, the scaling ratios were carefully determined. The geometric scale λ_L was estimated to be 1:300, deduced from the height of the maximum mean wind velocity (Z_{max} = 0.15m in the wind tunnel, corresponding to approximately 45 m in full-scale). The velocity scale λ_U was chosen as 1:3.9, considering a test velocity of 12 m/s versus a typical Andrews Air Force Base (AAFB) downburst velocity of 47 m/s [35]. Consequently, the time scale $\lambda_T = \frac{\lambda_L}{\lambda_U}$ is approximately 1:77. The simulated gust durations ($2\Delta T + \Delta t$) correspond to full-scale transient downburst events lasting approximately 38.5 s, 84.7 s, and 130.9 s, respectively.

2.2. Numerical Simulation

In the numerical simulation, the wind tunnel test section and the AMBS device are individually modeled according to their respective geometric dimensions, with the corresponding computational domain illustrated in Fig. (**3**). The cross-sectional area of the computational region matches that of the wind tunnel, and the static and dynamic blade rotation configurations are maintained in congruence with the wind tunnel experiments.

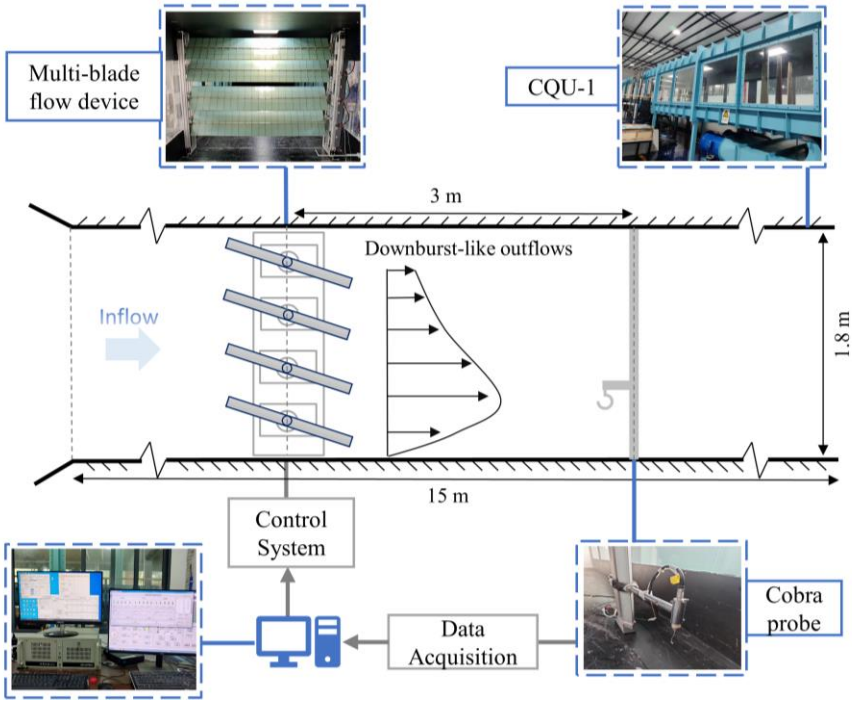

Figure 1: Active-controlled multi-blade system.

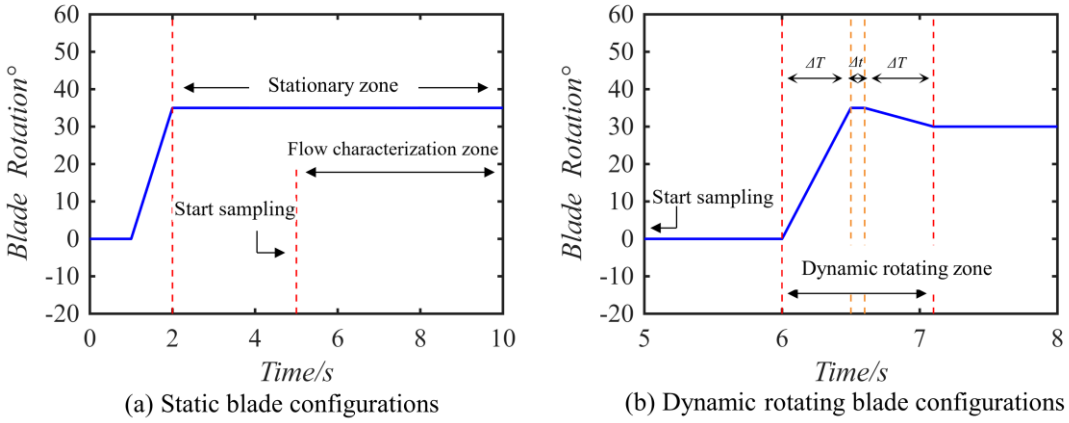

Figure 2: Rotating angle time history of the blades.

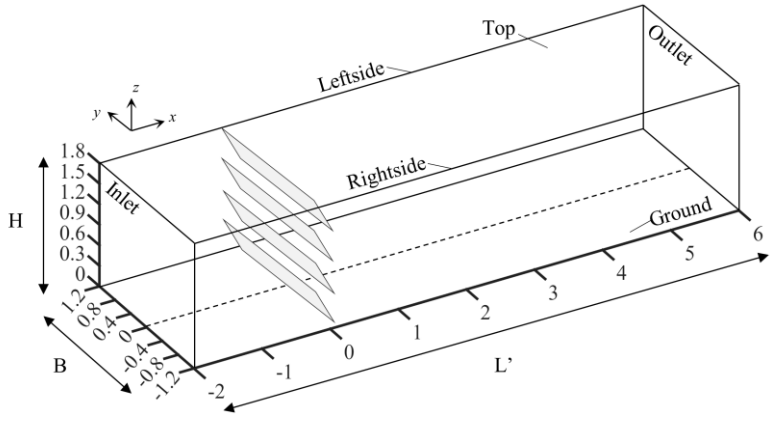

Figure 3: Computational domain diagram.

The multi-blade model is positioned at $x = 0\ m$, while the inlet and outlet boundaries were delineated at $x = -2\ m$ and $x = 6\ m$, respectively. The CFD simulations were carried out using Fluent 2024 R1. Within the computational domain, the stationary and moving zones were defined separately. The adjacent surfaces between these two regions were designated as interface boundaries to facilitate data exchange. By coupling the sliding mesh technique with User-Defined Functions (UDFs) in Fluent, the multi-blade array was driven to rotate dynamically within the flow field, thereby achieving the transient simulation of non-stationary downbursts. Regarding the boundary conditions, the downstream exit was set as a pressure outlet, while the left and right lateral boundaries were designated as symmetry planes. All remaining surfaces were specified as no-slip wall boundaries. At the inlet boundary, the fluctuating velocity components are generated using the CDRFG method [36] and subsequently superimposed onto the mean wind velocity profile. As shown in Fig. (**4a**), the computational domain was discretized using an unstructured mesh, with local grid refinements applied near the jet inlet, wall boundaries, and the multi-blade array to strictly control the dimensionless wall distance of the first grid nodes. The turbulence model employs large-eddy simulation, utilizing the SIMPLEC algorithm for velocity-pressure coupling to iteratively solve the discretized governing equations. For the spatial discretization, gradients were computed using the Least Squares Cell-Based method, momentum terms were discretized with the bounded central differencing scheme, and the pressure terms were solved using a Second Order scheme. A time step of 0.004 s was adopted, and the absolute convergence criterion was set to 1×10^{-5}. To assess grid independence, Fig. (**4b**) presents the mean velocity profiles at (x, y) = (3 m, 0 m) for three mesh resolutions (2.05 million cells, 4.30 million cells, and 6.50 million cells). The results indicate that further refinement yields only marginal changes in the velocity profile. To balance computational efficiency with rigorous accuracy, Mesh 2, comprising approximately 4.3×10^{6} cells, was selected for all subsequent analytical simulations.

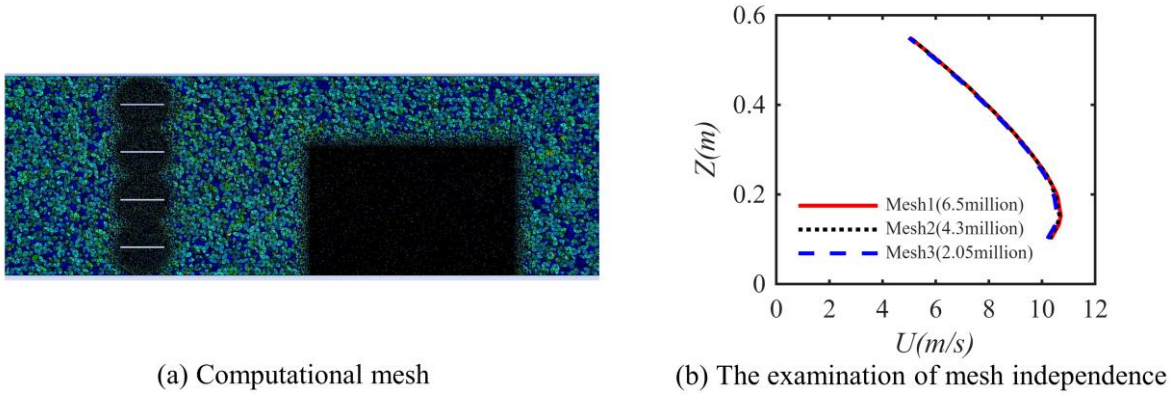

(a) Computational mesh (b) The examination of mesh independence

Figure 4: Computational mesh and the examination of mesh independence.

2.3. Wind Field Modelling

Fig. (**5a-d**) illustrates the wind velocity time histories derived from both experimental measurements and numerical simulations at the coordinate (x, y, z) = (3 m, 0 m, 0.15 m). To facilitate a granular examination of the subtle distinctions among non-stationary conditions characterized by varying gust durations, the figure displays only a 10-second segment of the data. It is evident that the simulated velocity time histories agree closely with the experimental results across all investigated cases. Under configurations utilizing an identical maximum blade rotation angle, the non-stationary cases exhibit the pronounced time-varying trends, with peak velocities significantly exceeding those observed in the stationary counterparts. Furthermore, the peak velocity within the nonstationary scenarios diminishes slightly as the gust duration extends. Fig. (**5e**) presents the probability density functions (PDFs) of the wind velocity time histories for both the stationary flow and the non-stationary flow with $\Delta T = 0.5s$. It is observed that the numerical results agree favorably with the experimental data. Specifically, the probability density under the stationary condition is highly concentrated, whereas it exhibits a broader dispersion under the non-stationary condition. These findings demonstrate that the numerical simulation can effectively replicate the wind tunnel measurements.

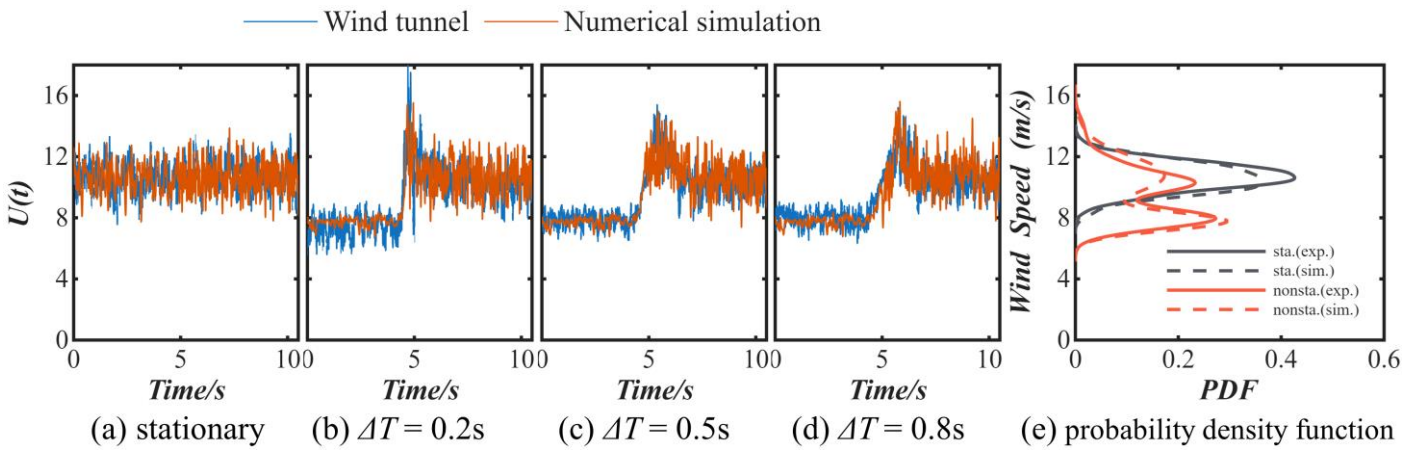

Figure 5: Time histories of wind velocities and corresponding probability density function.

2.3.1. Wind Speed Decomposition

To conduct a comprehensive analysis of the mean and fluctuating characteristics of the downburst wind field, the decomposition of the raw wind velocity time histories is as follows:

$$U(t) = \overline{U} + u(t) = \overline{U} + \sigma_u \tilde{u}(t) \tag{1}$$

Where $\overline{U}$ is the mean wind velocities, $u(t)$ is the residual fluctuations, $\tilde{u}(t) = u(t)/\sigma_u$ is the reduced fluctuations and σ_u denotes the standard deviation.

For stationary wind fields, statistical quantification can be achieved using the conventional constant mean and time-invariant standard deviation. In contrast, for nonstationary flows, owing to the transient duration and rapid velocity fluctuations inherent to downbursts, several techniques such as the moving average (MA), discrete wavelet transform, or empirical mode decomposition are required to extract the time-varying trend component [37-39]. In this study, the moving-average method is employed to extract the time-varying trend from the raw velocity. According to research by Solari [38], the decomposition can be considered effective when the correlation between the extracted mean component and the residual fluctuating component is minimal. To intuitively demonstrate the impact of different averaging periods on the separation quality, a correlation index between the mean and fluctuating components is introduced, defined by the following equation:

$$C_u = \int_0^\infty S_{\overline{U}(t)u(t)}(f)df \tag{2}$$

Where C_u is the degree of correlation between the time-varying average part and the residual fluctuation part, $S_{\overline{U}(t)u(t)}$ is the cross power spectral density function, f is the frequency vector. When C_u approaches zero, the low-frequency mean component and the high-frequency fluctuating component exhibit minimal spectral overlap within the frequency domain. Conversely, a larger of C_u value indicates a stronger correlation between the two components, resulting in suboptimal separation quality.

Fig. (**6**) illustrates the decomposition results for both stationary and non-stationary wind velocity time histories. As depicted in Fig. (**6a**), the efficacy of separating the mean and fluctuating components across varying moving averaging periods T is evaluated utilizing the aforementioned correlation index formula. It is evident that C_u decreases initially and then increases as T increases, reaching its minimum at $T = 0.3s$. Consequently, a moving period of 0.3 s was adopted in this study for the extraction of the time-varying mean wind velocity. As evidenced in Fig. (**6b**), the mean and root mean square values derived under the stationarity assumption remain time-invariant. In contrast, the corresponding statistics presented in Fig. (**6c**) manifest pronounced time-varying characteristics, exhibiting a marked increase during intervals of rapid wind velocity fluctuation.

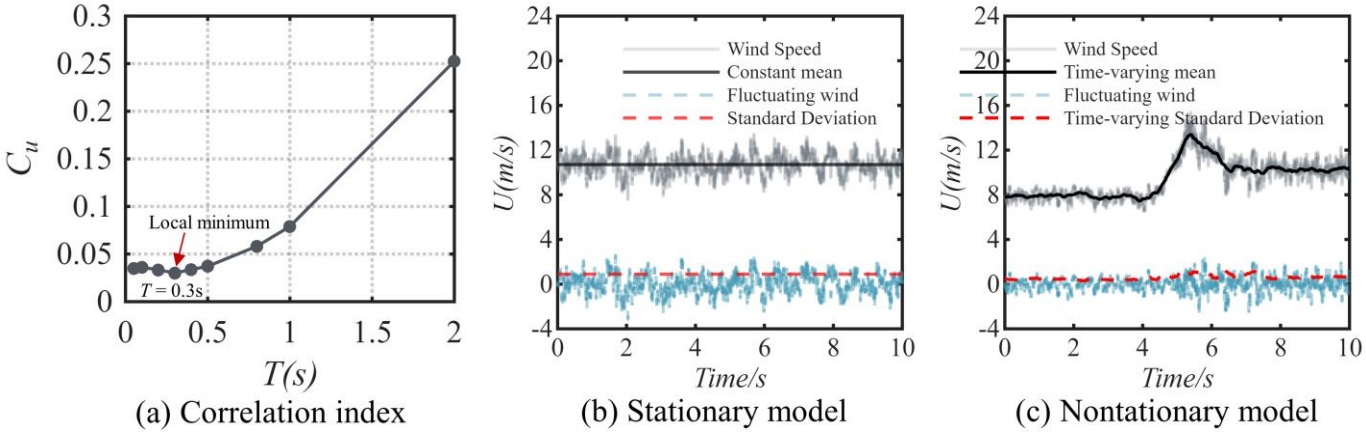

Figure 6: Stationary and nonstationary wind speed model.

2.3.2. Statistical Parameters of Turbulence Properties

Turbulence intensity and turbulence integral scale are critical parameters for representing the turbulence characteristics of the wind field. In the context of stationary flow, these parameters are defined by the following expressions:

$$I_u = \frac{\sigma_u}{\bar{U}} \tag{3}$$

$$L_u = \frac{\bar{U}}{\sigma_u^2}\int_0^{\infty} R_u(\tau)d\tau \tag{4}$$

Where I_u is the turbulent intensity, L_u is the turbulence integral scale, $R_u(\tau)$ denotes the auto-correlation function of fluctuating wind speeds. Under non-stationary conditions, the constant statistical value can introduce substantial errors in the assessment of turbulence parameters [40]. The mean wind speeds $\bar{U}$, standard deviation σ_u, and autocorrelation function $R_u(\tau)$ should be replaced with their time-varying counterparts.

The turbulent wind velocity spectrum characterizes the energy distribution of the fluctuating wind component $u(t)$ across the frequency domain. When $u(t)$ is regarded as a zero-mean stationary oscillatory process, the power spectral density (PSD) of $u(t)$ can be mathematically defined as the Fourier transform of the autocorrelation function:

$$S_u(\omega) = \frac{1}{2\pi}\int_{-\infty}^{+\infty} R_u(\tau)e^{-i\omega\tau}d\tau \tag{5}$$

For a zero-mean nonstationary stochastic process, the time-varying power spectral density, reflecting the magnitude of the contribution provided by distinct frequency components in the fluctuating wind at varying instants, can be estimated based on evolutionary power spectral density theory (EPSD) proposed by Priestley [41]. The EPSD is calculated as follows:

$$S_u(\omega, t) = \int_0^{+\infty} W(\tau)|\hat{u}(\omega, t-\tau)\hat{u}(\omega, t-\tau)^*|d\tau \tag{6}$$

$$\hat{u}(\omega, t) = \int_0^{+\infty} g(\tau)u(t-\tau)e^{-i\omega(t-\tau)}d\tau \tag{7}$$

$$g(\tau) = \begin{cases} \frac{1}{2\sqrt{h\pi}}, |\tau| \le h \\ 0, |\tau| > h \end{cases} \tag{8}$$

$$W(\tau) = \begin{cases} 1/\Gamma, -\frac{\Gamma}{2} \le \tau \le \frac{\Gamma}{2} \\ 0, otherwise \end{cases} \tag{9}$$

Where $\hat{u}(\omega,t)$ is the linear filtering signal of the stochastic process $u(t)$ at frequency ω. $S_u(\omega,t)$ is the estimated EPSD. $g(\tau)$ and $W(\tau)$ are the window functions and the weight function, respectively. The two key parameters of h and Γ are set as 25 dt and 105 dt respectively, and dt is the time step of $u(t)$.

3. Results and Discussions

3.1. Mean Wind Characteristics *of* Downburst Outflows

3.1.1. Wind Profiles for Stationary Cases

Fig. (**7a**) presents the vertical wind velocity profile of the stationary flows generated by the static blade configuration. It is founded that the experimental and simulation results exhibit remarkable consistency and the maximum mean velocity is approximately 10.7 m/s, occurring at a near-ground elevation of 0.15 m. The overall shape of the downburst-like outflow profile exhibits a pronounced nose-shaped characteristic, which diverges significantly from traditional atmospheric boundary layer (ABL) wind profiles that adhere to power-law or logarithmic laws. Furthermore, the empirical models of the vertical wind profile are included in the figure to verify the accuracy of the generated stationary wind field [42-44]. It is observed that the generated wind profile closely follows the Wood model [44] near the ground, while it aligns well with the Oseguera model [42] at higher elevations. To further validate the numerical predictions against the wind tunnel measurements, a correlation analysis is presented in Fig. (**7b**). The coefficient of determination (R^2) reaches 0.94, signifying a robust correlation. Meanwhile, the discrepancy between the simulated and experimental results is maintained within 10% for wind speeds ranging from 4 m/s to 12 m/s. This difference can be further quantified by the relative error $\varepsilon_U = \frac{\int_0^h |U_{\exp}(z) - U_{\mathrm{sim}}(z)| dz}{\int_0^h U_{\exp}(z) dz}$, where $U_{\exp}(z)$ is the experimental wind profile, $U_{\mathrm{sim}}(z)$ is the simulated wind profile, h denotes the maximum values of the height z. The analysis result shows that relative error ε_U is 6.46%, which is close to 5% and is considered acceptable. To compare against historical field measurements and prior wind tunnel experimental data [6, 27-29, 45-47], the results derived from this study are normalized with respect to the peak velocity U_{max} and its corresponding height Z_{max}, as shown in Fig. (**7c**). The comparison demonstrates that the present results fall within the range of the field data documented by Hjelmfelt [6] and align closely with wind profiles derived from other wind tunnel tests, thereby confirming the accuracy and reliability of the simulated wind profiles.

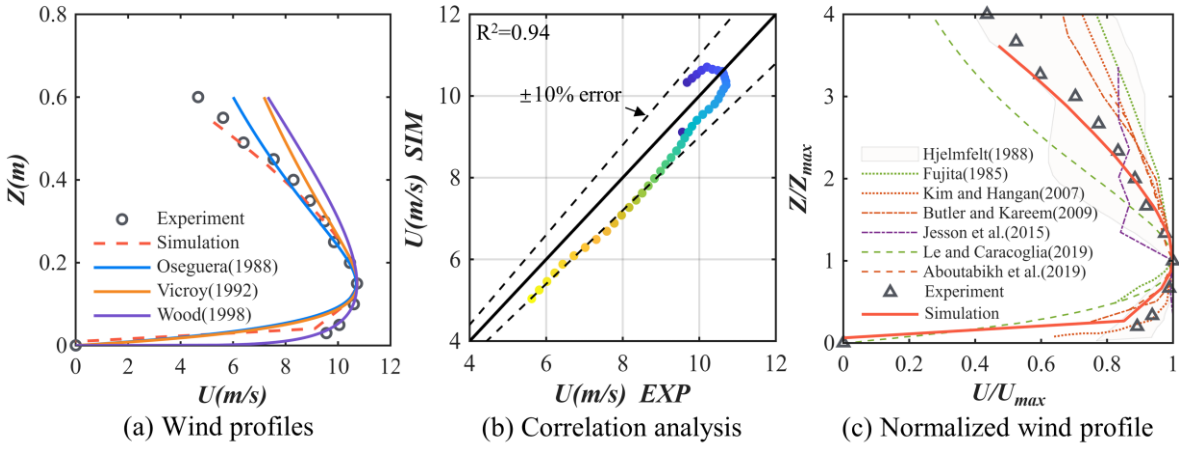

(a) Wind profiles (b) Correlation analysis (c) Normalized wind profile

Figure 7: Stationary wind profiles.

3.1.2. Evolutionary Wind Profiles for Nonstationary Cases

Fig. (**8a**) depicts the time histories of the time-varying mean wind velocity corresponding to downburst outflows with three distinct gust durations at a height of 0.15 m. It is observable that the dynamic blade-rotation configuration induces a marked surge in mean wind velocity. The transient variations in the wind field pose

substantial challenges to the estimation of aerodynamic loads based on quasi-steady theory [48]. Moreover, as the gust duration increases, the peak velocity of the nonstationary flow gradually decreases, accompanied by a delay in the occurrence of this peak. Such variations in duration may substantially influence the wind-induced responses of low-damping, highly flexible structures, such as tall buildings [34]. In practice, higher velocities variation rates do not necessarily induce greater wind loads. As demonstrated by Yan *et al*. [32], for wind turbine nacelle, the maximum overshoot ratio of wind pressure on the windward face frequently occurs at moderate wind speed acceleration. This phenomenon is likely attributable to cumulative effects. The transient nature of wind speeds typically results in lower structural responses due to the insufficient accumulation time required to reach steady-state values [49]. Therefore, conducting a statistical analysis of the overshoot ratios derived by wind pressures under non-stationary flows across various gust durations will significantly benefit the wind-resistant design of structures subjected to extreme wind events. To investigate the evolutionary characteristics of the vertical wind velocity distribution during non-stationary wind events, instantaneous velocity profiles are extracted for $\Delta T = 0.8s$ at six distinct time instances, ranging from 4 s to 7.6 s, as illustrated in Fig. (**8b**). At $t = 4\ s$, the boundary-layer profile follows an exponential law with its maximum velocity at the top. As time progresses, the height corresponding to the peak velocity descends, and by $t = 5.8\ s$ a pronounced nose-shaped profile emerges, with the maximum wind speed occurring near the ground. Conversely, during the subsequent velocity decay phase, the opposite trend is observed. The height of the peak velocity rises over time, until the wind velocity profile approaches uniformity at $t = 7.6\ s$. This entire evolutionary process of the wind profile bears a striking resemblance to previously documented field measurements of downburst events [50], thereby corroborating the validity of the simulated profiles. Furthermore, the spatiotemporal evolution characteristics of wind fields inherently induce variations in the load characteristics acting on structures and infrastructure. Such an analysis of the non-stationary wind environment is instrumental in elucidating the underlying causes and mechanisms governing the spatiotemporal variations of structural loads.

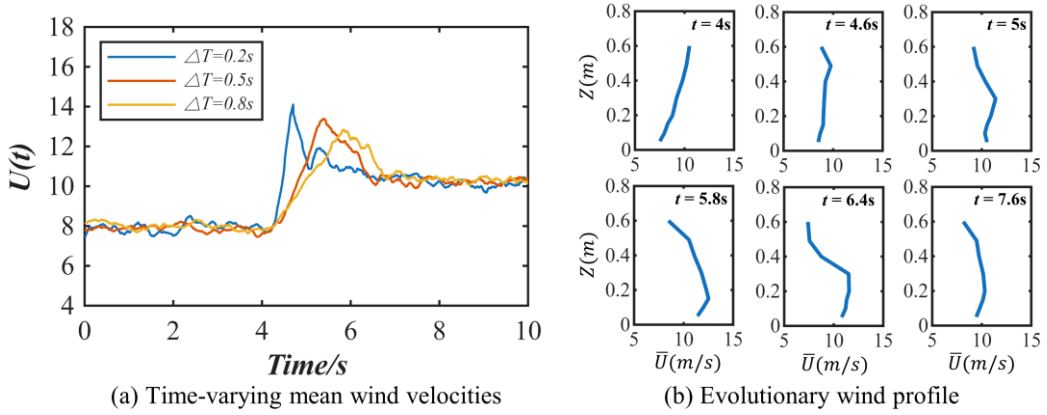

(a) Time-varying mean wind velocities (b) Evolutionary wind profile

Figure 8: Evolutionary features of wind profiles for nonstationary cases.

3.2. Fluctuating Wind Characteristics *of* Downburst Outflows

3.2.1. Probability Density Distribution

In structural wind load analysis, non-Gaussian characteristics significantly influence the transient extreme values of the loads. According to the studies by Li *et al*. [16, 18, 51], the strong non-stationary wind environment intensifies flow separation. The larger non-Gaussian peak factors are correlated with aerodynamic moments exhibiting highly non-stationarity. Therefore, the analysis of non-Gaussian features is crucial for the estimation of extreme wind loads. Fig. (**9a-c**) present the probability density functions (PDF) of the turbulent fluctuating components associated with both stationary and non-stationary flows, with the non-stationary case of $\Delta T = 0.5s$ selected as a representative example. The corresponding mean μ, standard deviation σ, skewness γ, and kurtosis κ are also provided for reference. The distributions of the fluctuating components derived from experimentation and simulation exhibit high consistency across all examined conditions, with mean values close to 0. The residual fluctuating components $u(t)$ of the stationary wind approximate a Gaussian distribution, whereas those of the nonstationary flow deviate markedly from Gaussian distribution. Their kurtosis coefficients marginally exceed 3,

thereby underscoring the pronounced non-Gaussian nature intrinsic to nonstationary downbursts. Compared with the Gaussian distribution, the results for the non-stationary flow align more closely with a double-exponential distribution, a finding consistent with observations from several field measurements [52, 53]. Furthermore, the PDF of the normalized fluctuating components $\tilde{u}(t)$, obtained by dividing by the standard deviation, largely follows a standard normal distribution, which is similar to that of the stationary condition. To examine the effect of gust duration on the non-Gaussian features of the residual turbulent fluctuating components, Fig. (**9d-f**) depict the PDFs corresponding to three gust-duration scenarios. It is evident that shorter gust durations correlate with elevated σ, γ, and κ, thereby indicating an intensification of non-Gaussian characteristics. Specifically, at $\Delta T = 0.2s$, the skewness marginally exceeds zero, while the kurtosis is substantially greater than 3. As the gust duration increases, both the kurtosis and skewness exhibit a significant decline, although a certain degree of non-Gaussian behavior persists. Across all three scenarios, the distributions of $u(t)$ distinctly follow a double-exponential distribution rather than a Gaussian distribution. The strong non-Gaussianity of such fluctuating winds significantly affects the estimation of extreme structural wind loads. For instance, Yan *et al*. [32] observed that the wind pressure peak factor on nacelle surfaces in accelerating flows is correlated with the wind speed acceleration, increasing as the acceleration decreases.

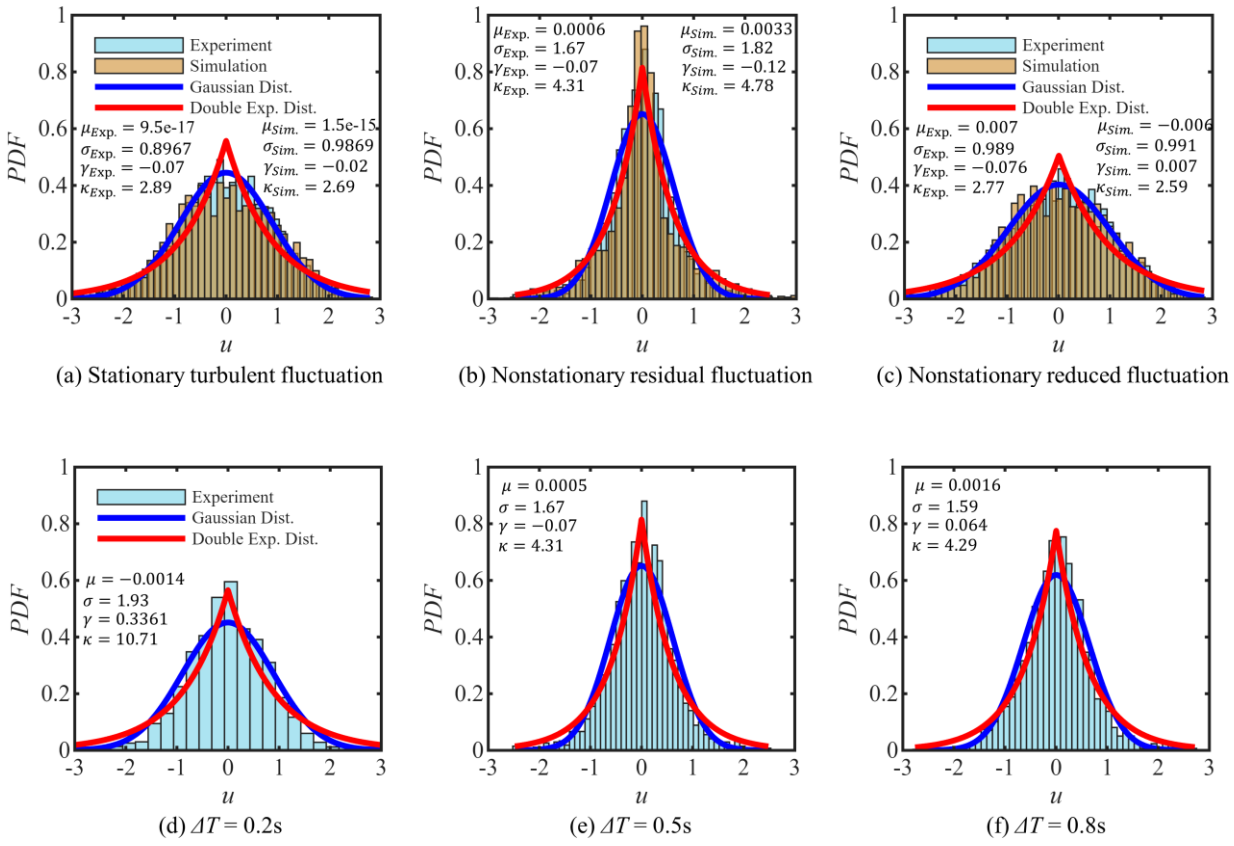

Figure 9: Probability density distribution of turbulent fluctuation at 0.15 m height.

3.2.2. Turbulence Intensity and Turbulence Integral Scale

Fig. (**10a**) illustrates the variation of turbulence intensity I_u with height for the stationary wind. The results demonstrate a favorable agreement between the experimental and numerical simulation. A comparison with the wind profile depicted in Fig. (**7**) reveals a clear negative correlation between turbulence intensity and mean wind velocity. Specifically, the turbulence intensity initially decreases and subsequently increases with height, reaching its minimum at the elevation corresponding to the maximum wind velocity. When compared with previous wind-tunnel studies [29, 54-57], the experimental and numerical results of the present work fall within the range reported by others, with turbulence intensities generally between 0.1 and 0.3. These values are also consistent with field measurements [38, 58], thereby confirming the reliability of the simulated turbulence levels.

Fig. (**10b**) depicts the temporal evolution of turbulence intensity I_u and the turbulence integral length scale L_u for both stationary and non-stationary flows at a height of z = 0.15 m. The stationary flow fails to capture the time-varying characteristics of the wind field parameters, as both its I_u and L_u remain constant. In contrast, the turbulence parameters for non-stationary flow exhibits significant transient surges, particularly during periods of rapid velocity change. Specifically, abrupt increases in I_u predominantly occur during the acceleration or decay phases of the wind speed, while a brief drop is observed when the velocity reaches its peak. Furthermore, the amplification of I_u diminishes as the gust duration lengthens, and by $\Delta T = 0.8s$, its variation becomes marginal, closely approaching the results observed in the stationary flow. Regarding the turbulence integral length scale L_u, its time-varying trend closely follows that of the time-varying mean wind velocity $\overline{U}$. The peak values of L_u across all three nonstationary conditions exceed those of the stationary flow, and exhibit a gradual reduction as the gust duration increases. This phenomenon, to a certain extent, reflects the inherent spatiotemporal variability of the downburst wind field.

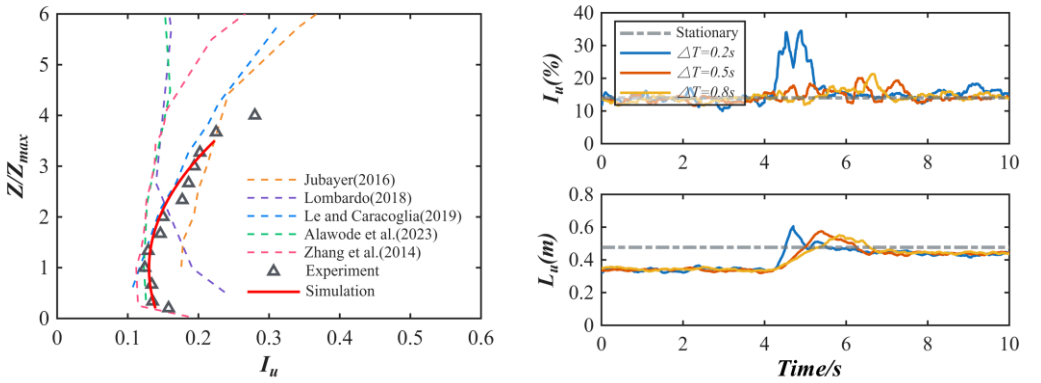

(a) Stationary turbulence intensity profiles (b) Nonstationary turbulence intensity and scale

Figure 10: Turbulence intensity and turbulence integral scale.

3.2.3. Turbulence Power Spectral Density

Fig. (**11a**) presents the power spectral density of the residual turbulent fluctuating components under stationary conditions. The numerically simulated fluctuating wind velocity spectra demonstrates close agreement with the wind tunnel experimental results in the low-frequency range and aligns well with the von Karman spectrum [59]. However, within the high-frequency range, a slight attenuation in the simulated spectral density is observed, indicating a certain degree of underestimation of the high-frequency part of velocity spectrum, which is attributable to the filtering of small-scale vortices inherent in the LES method. This phenomenon aligns with the findings of considerable previous studies [60, 61]. Fig. (**11b-c**) illustrate the wind velocity spectra corresponding to non-stationary flows characterized by two distinct gust durations. The evolutionary power spectra exhibit

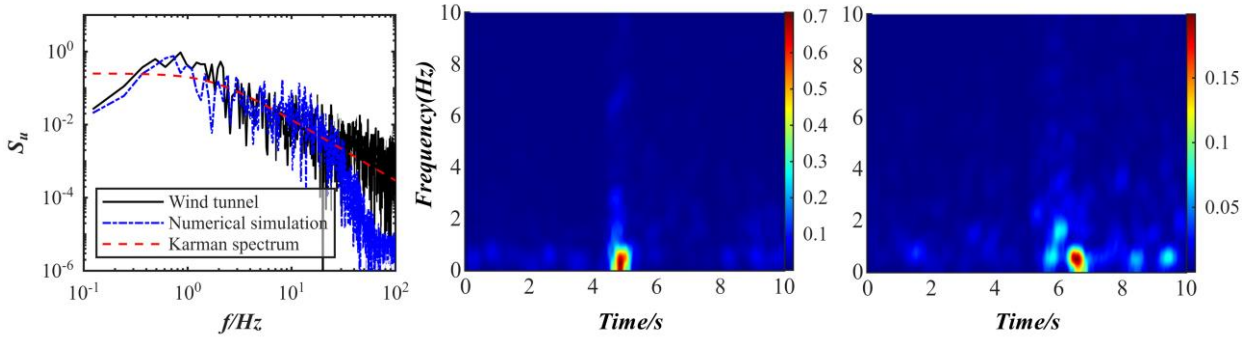

(a) Stationary PSD (b) ΔT = 0.2s (Nonstationary) (c) ΔT = 0.8s (Nonstationary)

Figure 11: Power spectral density of residual fluctuations.

pronounced time-varying characteristics at 0-2Hz, with higher spectral density values occurring during intervals of rapid velocity change. As the gust duration increases to $\Delta T = 0.8s$, the peak magnitude of the spectral density decreases, and its time of occurrence is correspondingly delayed. This phenomenon reflects the discrepancies in the distribution of turbulent energy within non-stationary wind fields.

4. Concluding Remarks

In this paper, stationary and non-stationary downburst-like flow fields are generated utilizing an active-controlled multi-blade device within both a boundary layer wind tunnel and a corresponding numerical simulation model. A comprehensive description and analysis are conducted regarding the wind profile characteristics, turbulence probability density distributions, turbulence intensities, turbulence integral scales, and fluctuating wind velocity spectra. The principal conclusions are summarized as follows:

1) By appropriately modifying a conventional boundary layer wind tunnel with a multi-blade system capable of modulating the outflow direction, two-dimensional downburst-like wind fields can be effectively simulated. Furthermore, Numerical simulations at the same geometric scale successfully reproduce analogous wind velocity time histories at different spatial locations.
2) In contrast to the time-invariant, nose-shaped vertical wind profile observed in stationary flows, the mean wind profile of non-stationary flows exhibits significant time-varying characteristics. Specifically, the altitude of the maximum velocity demonstrates a trend of initial descent followed by an ascent. Moreover, shorter gust durations are correlated with higher magnitudes of peak mean velocity.
3) The residual turbulent fluctuation of stationary flows predominantly adheres to a Gaussian distribution, whereas that of non-stationary flows aligns with a double-exponential distribution; however, the reduced fluctuating wind velocity conforms to a Gaussian distribution. Additionally, the non-Gaussian characteristics of non-stationary winds intensify as the gust duration decreases.
4) The turbulence intensity of the downburst initially decreases and subsequently increases with altitude, exhibiting a negative correlation with the mean wind velocity. Compared with the time-invariant turbulence parameters of stationary winds, the turbulence intensity and integral scales of non-stationary winds exhibit a marked augmentation during rapid variations in velocity. The magnitude of this amplification is negatively correlated with the gust duration.
5) Compared to the power spectrum of stationary winds, the evolutionary power spectral density of non-stationary winds manifests distinct time-varying features, wherein shorter gust durations are associated with larger spectral energy peaks.

Finally, the experimental and numerical simulation frameworks developed in this study for stationary and non-stationary downbursts can be widely applied to future research on structural wind effects. Specifically, these applications encompass various structures and infrastructure, such as low-rise buildings, high-rise buildings, and transmission towers. By subjecting target structures to simulated downbursts with varying wind profile shapes, velocity variation rates, and gust durations, the comprehensive analyses of aerodynamic coefficients, and wind-induced responses can be conducted. This will facilitate critical comparisons against current design code provisions derived from quasi-steady assumptions, thereby yielding profoundly instructive insights. These investigations will be systematically addressed in future works.

Conflict of Interest

The authors declare that they have no known competing financial interests or personal relationships that could have appeared to influence the work reported in this paper.

Funding

The work described in this paper was fully supported by a grant from the National Natural Science Foundation of China (Nos. 51978230 and 52278495) and the Natural Science Foundation of Anhui, China (No. 2108085J29).

Acknowledgments

The financial support is gratefully acknowledged by the authors.

Availability of Data and Materials

The data that support the findings of this study are available from the corresponding author upon reasonable request.

Author's Contributions

Zhipeng Wang: Investigation, Methodology, Formal analysis, Software, Writing – Original Draft, Writing – Review and Editing, Data Curation.

Lunhai Zhi: Conceptualization, Supervision, Formal analysis, Writing – Review and Editing, Project administration, Funding acquisition.

Bowen Yan: Project administration, Supervision, Resources.

Wei Guo: Software, Visualization.

References

[1] Mohee FM, Miller C. Climatology of thunderstorms for North Dakota, 2002–06. J Appl Meteorol Climatol. 2010; 49: 1881-90. https://doi.org/10.1175/2010JAMC2400.1

[2] Abd-Elaal ES, Mills JE, Ma X. A review of transmission line systems under downburst wind loads. J Wind Eng Ind Aerodyn. 2018; 179: 503-13. https://doi.org/10.1016/j.jweia.2018.07.004

[3] Kwon DK, Kareem A. Gust-front factor: new framework for wind load effects on structures. J Struct Eng. 2009; 135(6): 717-32. https://doi.org/10.1061/(ASCE)0733-9445(2009)135:6(717)

[4] Zhang H, Wang H, Xu Z, Zhang Y, Tao T, Mao J. Monitoring-based analysis of wind-induced vibrations of ultra-long stay cables during an exceptional wind event. J Wind Eng Ind Aerodyn. 2022; 221: 104883. https://doi.org/10.1016/j.jweia.2021.104883

[5] Fujita TT. Downbursts: meteorological features and wind field characteristics. J Wind Eng Ind Aerodyn. 1990; 36: 75-86. https://doi.org/10.1016/0167-6105(90)90294-M

[6] Hjelmfelt MR. Structure and life cycle of microburst outflows observed in Colorado. J Appl Meteorol Climatol. 1988; 27: 900-27. https://doi.org/10.1175/1520-0450(1988)027<0900:SALCOM>2.0.CO;2

[7] Simiu E. Estimation of wind effects on high-rise structures by the global load effects and database-assisted design methods. Int J Archit Eng Technol. 2025; 12: 1-7. https://doi.org/10.15377/2409-9821.2025.12.1

[8] Chen CW, Li YC, Lo YL. Interference effects on the square and circular cross-sectional high-rise buildings under turbulent flows. Int J Archit Eng Technol. 2022; 9: 18-36. https://doi.org/10.15377/2409-9821.2022.09.2

[9] Shakir I, Jasim MA, Weli SS. High rise buildings: design, analysis, and safety. Int J Archit Eng Technol. 2021; 8: 1-13. https://doi.org/10.15377/2409-9821.2021.08.1

[10] Solari G, Repetto MP, Burlando M, De Gaetano P, Pizzo M, Tizzi M, *et al*. The wind forecast for safety management of port areas. J Wind Eng Ind Aerodyn. 2012; 104-106: 266-77. https://doi.org/10.1016/j.jweia.2012.03.029

[11] McCarthy J. The classify, locate, and avoid wind shear (CLAWS) project at Denver's Stapleton International Airport: operational testing of terminal weather hazard warnings with an emphasis on microburst wind shear. In: Second International Conference on the Aviation Weather System; Montreal: 1985.

[12] Fujita TT. Objectives, operation, and results of Project NIMROD. In: Preprints of the 11th Conference on Severe Local Storms; 1979; Kansas City (MO). Boston: American Meteorological Society; 1979. p. 259-66.

[13] Solari G. Wind science and engineering: origins, developments, fundamentals and advancements. Cham: Springer; 2019.

[14] Yang L, Fang Z, Ma J, Jiao Y, Wang Z. Experimental investigation of downburst-induced wind loads on rectangular high-rise buildings: influence of geometric features. Phys Fluids. 2025; 37(8): 087132. https://doi.org/10.1063/5.0282050

[15] Ghazal T, Aboutabikh M, Aboshosha H, Abdelwahab M. Thunderstorm wind load evaluation on storm shelters using wind tunnel testing. Eng Struct. 2022; 262: 114350. https://doi.org/10.1016/j.engstruct.2022.114350

[16] Li X, Li S, Su Y, Peng L, Cao S, Liu M. Study on the time-varying extreme value characteristic of the transient loads on a 5:1 rectangular cylinder subjected to a thunderstorm-like wind. J Wind Eng Ind Aerodyn. 2022; 229: 105161. https://doi.org/10.1016/j.jweia.2022.105161

[17] Yan B, Yuan Y, Ma C, Dong Z, Huang H, Wang Z, *et al*. Modeling of downburst outflows and wind pressures on a high-rise building under different terrain conditions. J Build Eng. 2022; 48: 103738. https://doi.org/10.1016/j.jobe.2021.103738

[18] Li X, Li S, Li J, Su Y. Nonstationary time-varying extreme value of downburst-induced wind loads based on transformed stationary method. Probab Eng Mech. 2022; 70: 103345. https://doi.org/10.1016/j.probengmech.2022.103345

[19] Fang Z, Wang Z, Li Z, Yan J, Huang H. Wind field characteristics of stationary and moving downbursts based on the test of impinging jet with a movable nozzle. J Wind Eng Ind Aerodyn. 2023; 232: 105266. https://doi.org/10.1016/j.jweia.2022.105266

[20] Brusco S, Bin HY, Lo YL, Piccardo G. Transient aerodynamics of a square cylinder under downburst-like accelerating flows reproduced in a multiple-fan wind tunnel. J Fluids Struct. 2024; 124: 104038. https://doi.org/10.1016/j.jfluidstructs.2023.104038

[21] Canepa F, Romanic D, Hangan H, Burlando M. Experimental translating downbursts immersed in the atmospheric boundary layer. J Wind Eng Ind Aerodyn. 2023; 243: 105570. https://doi.org/10.1016/j.jweia.2023.105570

[22] Canepa F, Burlando M, Romanic D, Hangan H. Effect of surface roughness on large-scale downburst-like impinging jets. Phys Fluids. 2024; 36: 036610. https://doi.org/10.1063/5.0198291

[23] Romanic D, Ballestracci A, Canepa F, Solari G, Hangan H. Aerodynamic coefficients and pressure distribution on two circular cylinders with free end immersed in experimentally produced downburst-like outflows. Adv Struct Eng. 2021; 24: 522-38. https://doi.org/10.1177/1369433220958763

[24] Yan B, Peng Y, Cheng X, Ma C, Tian Y, Ji B, *et al*. A refined empirical model of steady-state downburst based on high-resolution wind speed data obtained from wind tunnel tests. Adv Wind Eng. 2024; 1: 100006. https://doi.org/10.1016/j.awe.2024.100006

[25] Li Y, Mason MS, Bin HY, Lo YL. Aerodynamic characteristics of a high-rise building in a steady thunderstorm outflow-like flow field. J Wind Eng Ind Aerodyn. 2023; 240: 105501. https://doi.org/10.1016/j.jweia.2023.105501

[26] Babu KBR, Hu G, Hong H, Lin P, Kwok KCS. Experimental investigation of wind-induced loading on a tall building under downburst-like outflow conditions. J Build Eng. 2026; 117: 114829. https://doi.org/10.1016/j.jobe.2025.114829

[27] Butler K, Kareem A. Characteristics of surface pressures on prismatic models in simulated gust front outflows. In: Proceedings of the 7th Asia-Pacific Conference on Wind Engineering; 2009; Tokyo. Tokyo: International Association for Wind Engineering; 2009.

[28] Aboutabikh M, Ghazal T, Chen J, Elgamal S, Aboshosha H. Designing a blade-system to generate downburst outflows at boundary layer wind tunnel. J Wind Eng Ind Aerodyn. 2019; 186: 169-91. https://doi.org/10.1016/j.jweia.2019.01.005

[29] Le V, Caracoglia L. Generation and characterization of a non-stationary flow field in a small-scale wind tunnel using a multi-blade flow device. J Wind Eng Ind Aerodyn. 2019; 186: 1-16. https://doi.org/10.1016/j.jweia.2018.12.017

[30] Yuan Y, Yan B, Zhou X, Li X, Yang Q, Zhou X, *et al*. An active-controlled multi-blade facility to generate 2-D downburst-like outflows in the boundary layer wind tunnel. J Wind Eng Ind Aerodyn. 2024; 248: 105713. https://doi.org/10.1016/j.jweia.2024.105713

[31] Yuan Y, Yan B, Zhou X, Li X, Dong Y, Yang Q, *et al*. Evolution of downburst-like flows produced by an active-controlled multi-blade facility. Phys Fluids. 2024; 36: 077152. https://doi.org/10.1063/5.0220379

[32] Yan B, Yuan Y, Zhou X, Li Y, Yang Q, Liu Q, *et al*. Experimental study of non-stationary aerodynamic effects on the wind turbine nacelles under extreme wind events. Phys Fluids. 2024; 36: 116103. https://doi.org/10.1063/5.0233895

[33] Wang Z, Zhi L, Yan B, Li Y. Assessment of wind effects on high-rise buildings by various aerodynamic modifications in a stationary downburst-like flow field. J Build Eng. 2026; 123: 115887. https://doi.org/10.1016/j.jobe.2026.115887

[34] Chen X. Analysis of multimode coupled buffeting response of long-span bridges to nonstationary winds with force parameters from stationary wind. J Struct Eng. 2015; 141(4): 04014131. https://doi.org/10.1061/(ASCE)ST.1943-541X.000107

[35] Holmes JD, Oliver SE. An empirical model of a downburst. Eng Struct. 2000; 22: 1167-72. https://doi.org/10.1016/S0141-0296(99)00058-9

[36] Aboshosha H, Elshaer A, Bitsuamlak GT, El Damatty A. Consistent inflow turbulence generator for LES evaluation of wind-induced responses for tall buildings. J Wind Eng Ind Aerodyn. 2015; 142: 198-216. https://doi.org/10.1016/j.jweia.2015.04.004

[37] Chen J, Wu M. On extraction of time-varying mean wind speed from wind record based on stationarity index. Asia Pac J Atmos Sci. 2012; 48: 315-23. https://doi.org/10.1007/s13143-012-0030-6

[38] Solari G, Burlando M, De Gaetano P, Repetto MP. Characteristics of thunderstorms relevant to the wind loading of structures. Wind Struct. 2015; 20: 763-91. https://doi.org/10.12989/was.2015.20.6.763

[39] Su Y, Huang G, Xu Y. Derivation of time-varying mean for non-stationary downburst winds. J Wind Eng Ind Aerodyn. 2015; 141: 39-48. https://doi.org/10.1016/j.jweia.2015.02.008

[40] Solari G. Thunderstorm response spectrum technique: theory and applications. Eng Struct. 2016; 108: 28-46. https://doi.org/10.1016/j.engstruct.2015.11.012

[41] Priestley MB. Evolutionary spectra and non-stationary processes. J R Stat Soc Ser B. 1965; 27(2): 204-37.

[42] Oseguera RM, Bowles RL. A simple, analytic 3-dimensional downburst model based on boundary layer stagnation flow. NASA Tech Memo. 1988; 100632.

[43] Vicroy DD. Assessment of microburst models for downdraft estimation. J Aircr. 1992; 29: 1043-8. https://doi.org/10.2514/3.46282

[44] Wood GS, Kwok KCS, Motteram NA, Fletcher DF. Physical and numerical modelling of thunderstorm downbursts. J Wind Eng Ind Aerodyn. 2001; 89: 535-52. https://doi.org/10.1016/S0167-6105(00)00090-8

[45] Fujita T. The downburst-microburst and macroburst report of projects NIMROD and JAWS. Chicago: University of Chicago; 1985.

[46] Kim J, Hangan H, Ho TC. Downburst versus boundary layer induced wind loads for tall buildings. Wind Struct. 2007; 10: 481-94. https://doi.org/10.12989/was.2007.10.5.481

[47] Jesson M, Sterling M, Letchford C, Haines M. Aerodynamic forces on generic buildings subject to transient, downburst-type winds. J Wind Eng Ind Aerodyn. 2015; 137: 58-68. https://doi.org/10.1016/j.jweia.2014.12.003

[48] Kwon DK, Kareem A. Generalized gust-front factor: a computational framework for wind load effects. Eng Struct. 2013; 48: 635-44. https://doi.org/10.1016/j.engstruct.2012.12.024

[49] Chen X. Analysis of alongwind tall building response to transient nonstationary winds. J Struct Eng. 2008; 134(5): 782-91. https://doi.org/10.1061/(ASCE)0733-9445(2008)134:5(782)

[50] Solari G, Burlando M, Repetto MP. Detection, simulation, modelling and loading of thunderstorm outflows to design wind-safer and cost-efficient structures. J Wind Eng Ind Aerodyn. 2020; 200: 104142. https://doi.org/10.1016/j.jweia.2020.104142

[51] Li X, Li S, Yang Q, Hui Y, Cao S. Time-varying up-crossing theory-based non-stationary extreme estimation of gust-loading on rectangular cylinder due to thunderstorm-like wind. Probab Eng Mech. 2023; 74: 103506. https://doi.org/10.1016/j.probengmech.2023.103506

[52] McCullough M, Kwon DK, Kareem A, Wang L. Efficacy of averaging interval for nonstationary winds. J Eng Mech. 2014; 140: 1-19. https://doi.org/10.1061/(ASCE)EM.1943-7889.0000641

[53] Liu M, Pan Y, Hu J, Zhang C, Yu X, Xie Z. Field measurement study of intense thunderstorm outflows characteristics based on 356 m high meteorological tower. J Wind Eng Ind Aerodyn. 2023; 242: 105590. https://doi.org/10.1016/j.jweia.2023.105590

[54] Jubayer C, Elatar A, Hangan H. Pressure distributions on a low-rise building in a laboratory simulated downburst. In: Proceedings of the 8th International Colloquium on Bluff Body Aerodynamics and Applications (BBAA VIII); 2016 Jun 7-11; Boston (MA).

[55] Lombardo FT, Mason MS, de Alba AZ. Investigation of a downburst loading event on a full-scale low-rise building. J Wind Eng Ind Aerodyn. 2018; 182: 272-85. https://doi.org/10.1016/j.jweia.2018.09.020

[56] Alawode KJ, Azzi Z, Elawady A, Chowdhury AG. Dynamic properties of an aeroelastic transmission tower subjected to synoptic and downburst-like outflows. J Wind Eng Ind Aerodyn. 2023; 242: 105557. https://doi.org/10.1016/j.jweia.2023.105557

[57] Zhang Y, Sarkar P, Hu H. An experimental study on wind loads acting on a high-rise building model induced by microburst-like winds. J Fluids Struct. 2014; 50: 547-64. https://doi.org/10.1016/j.jfluidstructs.2014.07.010

[58] Choi ECC. Wind characteristics of tropical thunderstorms. J Wind Eng Ind Aerodyn. 2000; 84: 215-26. https://doi.org/10.1016/S0167-6105(99)00054-9

[59] von Kármán T. Progress in the statistical theory of turbulence. Proc Natl Acad Sci U S A. 1948; 34: 530-9. https://doi.org/10.1073/pnas.34.11.530

[60] Li Y, Zhu Y, Chen F, Li QS. Aerodynamic loads of tapered tall buildings: insights from wind tunnel test and CFD. Structures. 2023; 56: 104975. https://doi.org/10.1016/j.istruc.2023.104975

[61] Yan B, Ran Q, Yuan Y, Ren H, Li X, Zhou X, *et al*. Numerical investigation on the twisted wind-induced aeroelastic response of a square supertall building. J Fluids Struct. 2025; 137: 104350. https://doi.org/10.1016/j.jfluidstructs.2025.104350